TU Delft

Delft University of Technology

Does early age creep influence buildability of 3D printed concrete? Insights from numerical simulations

Chang, Ze; Liang, Minfei; Chen, Yu; Schlangen, Erik; Šavija, Branko

DOI
10.1016/j.addma.2023.103788

Publication date
2023

Document Version
Final published version

Published in
Additive Manufacturing

Citation (APA)
Chang, Z., Liang, M., Chen, Y., Schlangen, E., & Šavija, B. (2023). Does early age creep influence buildability of 3D printed concrete? Insights from numerical simulations. *Additive Manufacturing* , *77*, Article 103788. https://doi.org/10.1016/j.addma.2023.103788

Important note
To cite this publication, please use the final published version (if applicable).
Please check the document version above.

Copyright
Other than for strictly personal use, it is not permitted to download, forward or distribute the text or part of it, without the consent of the author(s) and/or copyright holder(s), unless the work is under an open content license such as Creative Commons.

Takedown policy
Please contact us and provide details if you believe this document breaches copyrights.
We will remove access to the work immediately and investigate your claim.

This work is downloaded from Delft University of Technology.
For technical reasons the number of authors shown on this cover page is limited to a maximum of 10.

Additive Manufacturing 77 (2023) 103788

Contents lists available at ScienceDirect

Additive Manufacturing

journal homepage: www.elsevier.com/locate/addma

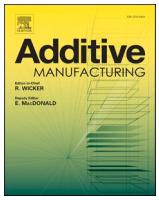

Does early age creep influence buildability of 3D printed concrete? Insights from numerical simulations

Ze Chang *, Minfei Liang, Yu Chen, Erik Schlangen, Branko Šavija

Microlab, Faculty of Civil Engineering and Geosciences, Delft University of Technology, 2628 CN Delft, the Netherlands

ARTICLE INFO

Keywords:
Early-age creep
Buildability quantification
Lattice model
Local force method

ABSTRACT

Cementitious materials may exhibit significant creep at very early age. This is potentially important for concrete 3D printing, where the material is progressively loaded even before it sets. However, does creep actually affect the buildability of 3D printed concrete? Herein, the influence of early-age creep on the buildability of 3D printed concrete is studied numerically. Creep is considered using the "local-force method", which was developed in our previous work. This 3D printing model be used to quantify the influence of early-age creep on typical failure modes, i.e., structural instability due to buckling and plastic collapse resulting from material yielding. The green strength and early-age creep experiments are conducted to characterize early-age visco-elastic-plastic behaviors. The model is then validated with the comparison to printing experiment about buildability quantification and failure mode prediction. Parametric analyses are subsequently performed to quantify the influence of early-age creep on various printing geometries in which different failure modes are dominant. The numerical results highlight the significance of initial printing time and material mix design for predicting the buildability of 3D printing of concrete. Finally, a discussion on how creep affects structural buildability is given from the perspective of localized damage and element strain.

1. Introduction

3D concrete printing (3DCP) is one of the most widely used digital fabrication methods in construction [1,2]. This advanced technology enables to construct the computer-designed structures via a layer-by-layer extrusion process. Contrary to conventional construction methods, 3DCP can do away with or significantly reduce the need for formwork, thereby decreasing the labor and construction costs [3]. In addition, this technique could enhance the safety and health of construction workers, especially under harsh conditions.

3DCP has been employed in a wide range of applications, from individual building components to full-scale architectural design [1,4,5]. Typical examples consist of the Dutch bicycle bridge, Dubai office building, and several 3D printed structures in China, the Middle East and the USA [1]. These projects show the construction industry's interest in this automation manufacturing technology. However, full adoption in the construction sector is still far away due to the lack of knowledge regarding material properties and structural behaviour in the fresh state.

In most cases, a trial-and-error approach is commonly utilized for printing scheme design. Successful printing can be guaranteed through a series of trials; however, this means high time and labor cost. Strong reliance on printing trials is caused by a lack of reliable numerical or analytical models for structural analysis of 3DCP [6]. As a result, such experiments are the only feasible option in relation to the printing geometry and material mix design. To tackle this issue, analytical or numerical tools must be developed to simulate the printing process and quantify buildability [7].

In 3DCP, the entire printing process consists of the pumping, extrusion, and build-up stages. During the printing process, several criteria including the pumpability, extrudability and buildability, are generally adopted to describe the material behaviors [8]. These evaluation criteria are based on the relevant theories which include fluid mechanics, rheology, and solid mechanics, as described in Fig. 1. During the pumping process, the cementitious materials subjected to the stress higher than the yield stress behave roughly like visco-plastic Bingham materials. In pursuit of good pumpability, the printable materials should be conveyed in the pipe smoothly without any blockages. Computational fluid dynamics (CFD) models based on the fluid mechanics have

* Corresponding author.
E-mail addresses: z.chang@tue.nl, z.chang-1@tudelft.nl (Z. Chang), M.Liang-1@tudelft.nl (M. Liang), Y.Chen-6@tudelft.nl (Y. Chen), Erik.Schlangen@tudelft.nl (E. Schlangen), b.savija@tudelft.nl (B. Šavija).

https://doi.org/10.1016/j.addma.2023.103788
Received 27 February 2023; Received in revised form 3 September 2023; Accepted 13 September 2023
Available online 15 September 2023
2214-8604/© 2023 The Author(s). Published by Elsevier B.V. This is an open access article under the CC BY license (http://creativecommons.org/licenses/by/4.0/).

been used to investigate the effect of constitutive relationships (such as generalized Newtonian fluid and elasto-visco-plastic fluid) on the cross-sectional geometry of a printed layer [9]. Furthermore, the relationship between the layer geometry and a series of printing parameters, including printing velocity and nozzle height, is studied as well [6,10,11]. CFD models can describe the filament instability and tearing induced by the imbalanced speed between the nozzle movement and the material flow, enabling the design of an optimal extrusion process [11]. However, the majority of CFD models focus on the extrusion process or a single-layer geometry; and not on structural buildability after material deposition.

Given that 3D printable cementitious materials are visco-plastic during the pumping process, rheological behaviors may affect material printability, comprising of the pumpability and extrudability. Roussel presented analytical models on the basis of rheology to evaluate the material behaviour during printing process [13]. These models analyzed the structural failure at the fresh stage considering the material yielding and buckling failure [13]. He also proposed criteria to evaluate the rheological requirements and examine the final geometrical dimensions of a single layer, considering also surface cracking and structural instability. Further investigations into thixotropy or other rheological properties have been conducted [14–21]. These models are mainly used to characterize the extrusion and pumping processes from the standpoint of material rheology. Some studies also attempt to use analytical methods to quantify structural build-up while the geometry characteristic and structural heterogeneity are difficult to be considered [18,22–26].

Material rheology is more accurate to describe the material behaviour during printing process from the perspective of chemical reaction and physical origin. However, some simplified terminologies like 'elastic buckling' and 'plastic collapse', which accounts for the impact of geometry on structural failure, have been widely used by the researchers in 3DCP. Associated with the 'elastic buckling' and 'plastic collapse', solid mechanics-based mathematical or numerical tools have been suggested for buildability quantification and prediction of structural deformation. A mechanistic model presented by Suiker [27] considers the effects of time-dependent material properties, printing velocity, boundary conditions, imperfections, and non-uniform gravitational loading. This model can simulate elastic buckling and plastic collapse of a wall structure [27–29]. The primary advantages of this model lie in its simplicity and time efficiency. However, this mechanistic model has the same limitation as analytical models. In addition, Suiker's model is not applicable to other printing geometries. To better understand the structural failure during printing process, finite element (FE) models have been developed to quantify the structural buildability, using the time-dependent material properties and Mohr-Coulomb failure criterion as inputs [28,30,31]. These models can reproduce the typical failure modes (i.e., elastic buckling and plastic collapse). However, the numerical results and experimental data are not in agreement due to neglection of localized damage, non-uniform gravitational loading, and deformed printing geometry. Some of these effects have been studied in other FE models [32–34] and other novel methods [12,33,35,36]. For instance, all aforementioned factors have been considered in a lattice-type model used to assess the plastic collapse-type failure during printing. A good quantitative agreement between the modelling results and experimental findings was reported [37]. Furthermore, the lattice model with geometric nonlinearity can reproduce the experimentally derived failure mode (i.e., asymmetric buckling) without introducing geometric imperfections [38].

So far, numerical models have shown good potential in predicting buildability and structural deformation of 3DCP. However, in most 3DCP models based on solid mechanics, the material is assumed to be elasto-plastic. This implies that only instantaneous strain is considered during the printing process, while time-dependent deformation is neglected. This time-dependent deformation increases with printing time, and comprises basic creep, plastic and autogenous shrinkage, and consolidation settlement. Herein, the terminology 'early-age' is used for the description of this kind of time-dependent deformation. According to the published research, several early-age creep tests of 3D printable paste/mortar have been proposed [39,40]; experimental results indicate that early-age creep makes for about 2% viscoelastic strain [40]. Therefore, early-age creep needs to be incorporated into 3D printing model to explore its effects on the buildability quantification. A chemo-mechanical FE model [34] has been proposed to account for several important features of the printable cementitious, including early-age creep, plasticity and aging due to hydration. In particular, hydration is described by a modified affinity hydration model. This chemo-mechanical model with the consideration of damage-plasticity theory was used to study the impact of hydration degree and early-age creep on the buildability quantification of 3DCP. However, no actual measurements of early-age creep were available; consequently, the creep compliance functions used in the model do not correspond to any real 3D printable cementitious material. This makes it impossible to determine the quantitative effects of creep in 3DCP. In addition, the interaction between the early-age creep and localized damage (i.e., material yielding) during the printing process has not been previously considered. Therefore, further investigation into how early-age creep affects build-up stage of 3DCP is required.

Here, the lattice model considering geometric nonlinearity and using an incremental algorithm [38] is extended to investigate the impact of early-age creep on structural analysis of 3DCP. The tested results from uniaxial compression experiment and early-age creep experiment are used to calibrate the input material properties [41]. The model is then validated by comparison with an experiment in which a wall structure is 3D printed. The quantitative effect of early-age creep on structural analysis is determined through parametric analyses. In the end, an explanation of how creep affects structural buildability is given from the perspective of localized damage and creep strain. This work primarily focuses on using numerical methods to quantify the impact of early-age creep on buildability and explain the mechanism of structural failure. The previously conducted experiments [41] were used to calibrate the material properties for the numerical model.

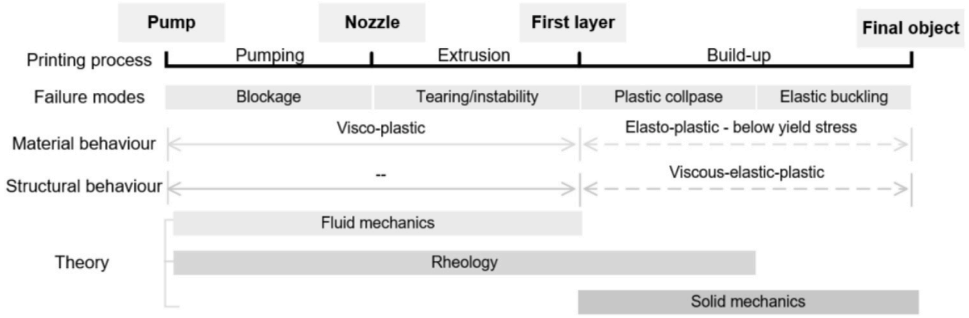

Fig. 1. Schematic diagram of 3D concrete printing at different stages [12].

2. Methods

In 3DCP, the mechanical stresses increase non-uniformly due to the gravitational loading caused by the continuous extrusion process. At some point in time, the printing geometry may fail due to plastic collapse because of the material yielding or structural instability induced by elastic buckling. These two failure modes can be reproduced by the 3D printing lattice model developed by the authors [12,37,38], as shown in Fig. 2. This section will review the model scope, main procedures and assumptions of this model.

2.1. Model scope

In light of the significant ratio of early-age creep to elastic deformation, it may exert adverse effects on structural buildability during the printing process. To quantify this influence and gain a comprehensive understanding of how early-age creep affects structural buildability, this study integrated experimentally derived early-age creep into a 3D printing model. Since the lattice model enables us to accurately investigate structural behavior and account for damage, the lattice model is therefore used as the basic model to study the coupled effect of damage and creep deformation on structural failure.

In this study, it's important to note that our current research primarily focuses on quantifying the effects of creep on buildability, with the mechanisms of early-age creep generation beyond the scope of this study. For future investigations, we recommend integrating a chemical hydration model with a 3D printing model to elucidate the underlying mechanisms from the perspective of chemical reactions at a micro-scale. This would provide valuable insights into the intricate interplay between material properties and structural behavior during the printing process.

2.2. Model description

For model generation, the continuum domain containing the designed printing geometry is first divided into a series of cells, each of which contains a sub-cell. The size of cell is defined as mesh resolution in this study. This domain is schematized by randomly generated lattice nodes within sub-cells, each of which takes one Voronoi cell. Nodal forces are calculated based on the volume of the Voronoi cell. Delaunay triangulation is then used to connect these lattice nodes to discretize the analyzed object using Timoshenko beams, which can transfer normal forces, shear forces, bending, and torsion.

In the 3D printing model, the single printing layer is composed of several printed segments to account for the continuous printing process. During numerical analysis, these printing segments are activated as the printing time increases. Therefore, the impact of non-uniform gravitational loading can be considered for structural analysis of 3DCP.

For buildability quantification, the analyzed object is subjected to a load increment at each step of the analysis. The lattice elements in which stresses are higher than the strength (i.e., tensile or compressive strength) will be marked as localized damage and removed from the lattice mesh. The numerical analysis for buildability quantification continues until the subsequent printing segment cannot be positioned on the deformed geometry; in other words, when the difference between the designed and actual positions is larger than the layer width. After that, the critical printing layer is determined, as well as the deformed shape and failure mode.Fig. 3.

2.3. Model limitations

This proposed model can reproduce two typical failure modes (i.e., elastic buckling and plastic collapse) of the printing system in the fresh stage. Possible cold joints and plastic shrinkage caused by water loss and relative humidity are not considered. This model adopts the basic theory of solid mechanics. In this study, the material properties are assumed to be visco-elastic-plastic. The green strength test can be used to identify the plastic behaviour of printed materials, whereas the early-age creep test enables the determination of viscous-elastic characteristics [41]. The current 3D printing model is based on solid mechanics, which means that parameters associated with the rheological properties, such as the complex shear modulus used to characterize viscoelastic behavior, cannot be considered.

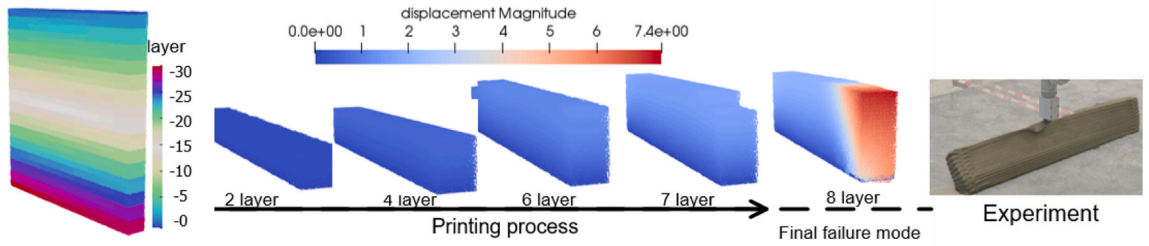

(a)

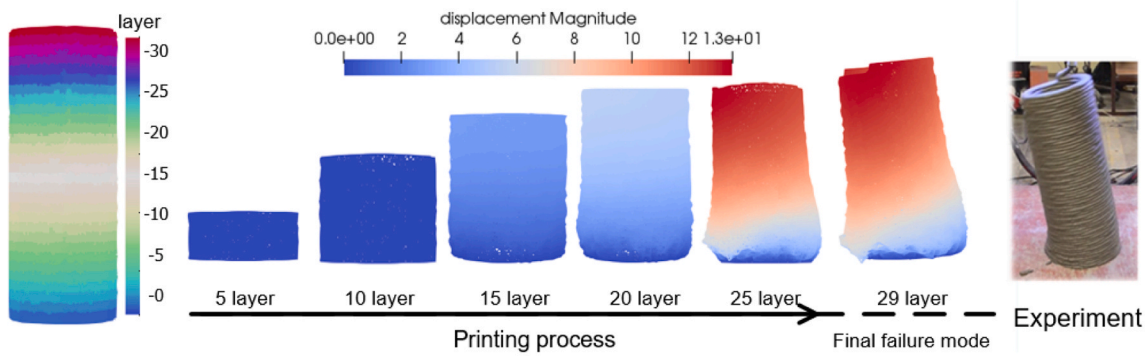

(b)

Fig. 2. Structural failure modes during printing process (a) elastic buckling [28] (b) plastic collapse [12,26].

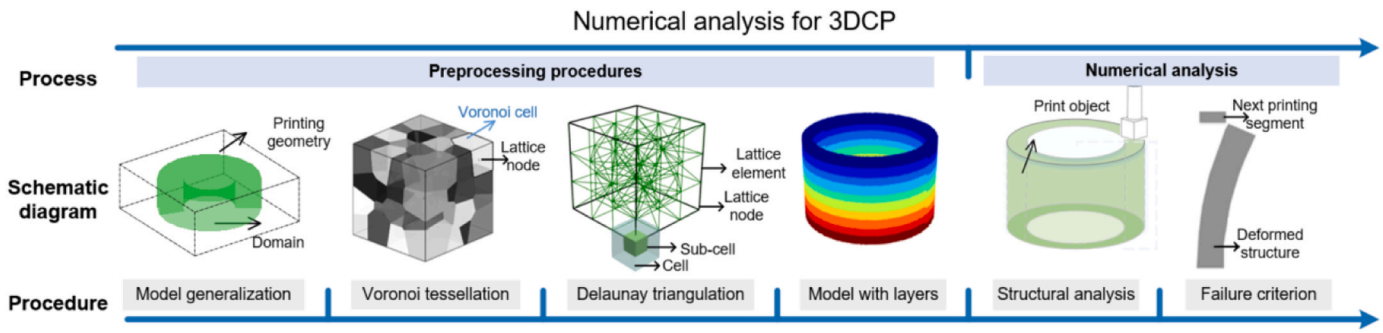

Fig. 3. A schematic diagram for numerical analysis for 3DCP using lattice model [37].

3. Theory

In our previous research, a 'local force method' for simulating early-age creep of cementitious materials under different loading conditions (i.e., constant, loading and unloading) has been proposed [42]. In this approach, the creep strains of lattice elements are first computed using the element stresses and creep compliance as input. These are then converted into forces which are applied in lattice beam elements. Herein, the 3D printing model [38] for elastic buckling and plastic collapse simulation is extended to investigate the influence of early-age creep on buildability quantification. The detailed procedures for model implementation of early-age creep will be introduced in this section.

3.1. Theoretical framework

3.1.1. Creep analysis

Creep refers to a strain/deformation increase at a constant stress level. The creep is a kind of time-dependent deformation due to alteration of material structures [43–46]. A superposition principle has first been presented by Boltzmann and improved by Volterra to describe creep of cementitious materials [45]. According to the linear viscoelastic model, the creep response can be superimposed based on several individual loading histories. The creep strain of each element can be calculated using Eq. (1), with the creep compliance and loading history as inputs. Subsequently, these strains are converted into element forces and applied to the numerical model. The time-dependent deformation can be modelled using this 'local force method', which is similar to the effective elastic modulus method proposed by Bažant [47–49]. In contrast to the effective elastic modulus method, this solution method requires no approximation of the creep constitutive law and can exactly reproduce the analytical model [42].

$$\varepsilon(t) = \sum_{i=1}^{i=N} \Delta\sigma(\tau_i) J(t-\tau_i, \tau_i)$$
$$J(t-\tau_i, \tau_i) = 1/E(\tau_i) + C_0 C_1(\tau_i) C_2(t-\tau_i) \quad (1)$$

in which $\Delta\sigma$ refers to incremental stress in each loading step; C_0 is the creep coefficient associated with material properties and other environmental factors such as temperature and relative humidity (RH); C_1 describes the influence of aging/hardening time (τ) on the prediction of creep compliance through the form of a power law function; C_2 studies the influence of the non-aging/loading duration (t-τ) on the creep compliance determination using another power law function [50,51].

Note that the superposition principle only holds true if each loading step is independent. It means that the previous loading conditions do not affect on the creep response for the following loading periods. If the principle stress is higher than the 40–50% of the material strength [52,53], damage may occur, resulting in non-linear creep response [53]. To simulate the creep behaviour under high loading level, the superposition principle would need to be combined with a damage law [47,54]; in the current study, the element removal approach is used.

3.1.2. Numerical algorithm

In this section, the local force method will be incorporated into the previously developed 3D printing model based on the incremental algorithm with geometric nonlinearity [37,38]. Here, a brief overview of this numerical algorithm will be given, and the detailed information can be found in [38]. To perform the structural analysis of 3DCP, the virtual displacement formulation and second-order elastic analysis are used to derive the basic equation, which is expressed as follows.

$$(K_t + K_g)\Delta D = \Delta F$$
$$\Delta F = F_{ex} - F_{in} \quad (2)$$

in which ΔF and ΔD are disequilibrium force and displacement of the analyzed model. The kind of force can be calculated using the external load F_{ex} and internal element force F_{in}. The K_t, (i.e., material stiffness matrix) and K_g (i.e, geometric stiffness matrix) are used to account for the material behaviour and geometric nonlinearity.

3.2. Model implementation

The section describes the detailed procedures on how to incorporate the local force method into the 3D printing model for structural analysis during the printing process. The numerical implementation consists of seven steps: A, B, C, D, E, F and G, as shown in Fig. 5.

In the schematic diagram, k and K refer to the local and global system stiffness matrix, which consists of material stiffness k_t/K_t and geometric stiffness k_g/K_g. The superscript 'i' stand for the printing time, which determines the viscoelasticity material property and gravitational loading from the activated printing segments.

3.2.1. Step A: Model generalization

To build a lattice model for structural analysis of 3DCP, the continuum domain is first discretized by a group of lattice nodes, which is connected through beam elements. The designed geometry is obtained via the mapping procedure, as described in Section 2.1. After that, a 3D printing model is well prepared for the numerical analysis of 3DCP.

3.2.2. Step B: material properties determination

Given that 3D concrete printing is a time-dependent process, the material behaviors of each printed segment differ from the hydration time and position. The material properties of lattice elements can be determined with the printing time and time-strength curve as inputs.

3.2.3. Step C: structure analysis of printed segments

The transient material properties are used in this model to compute the material stiffness matrix. The geometric stiffness is computed using the stored element forces, and the detailed procedures can be found in [38]. The numerical equation, subject to incremental loading, can be solved using the Runge-Kutta method to get the structural response. The computed element stresses are then used as incremental stresses for creep strain computation. The derived incremental displacement is utilized to update the printing geometry.

3.2.4. Step D: local force computation

With the known creep compliance and stored element stress as inputs, the creep strain of lattice elements can be derived, as expressed in Eq. (1). Subsequently, these computed strains are transferred into axial forces, which refers to the local force in this study. Given that this numerical analysis adopts the incremental solution, the difference about creep force between two steps are then calculated, as described in Eq. (3).

$$\begin{aligned} \sigma_{cr,i} &= E\varepsilon_{cr,i} \\ f_{cr,i} &= \sigma_{cr,i}A \\ \Delta f_{cr,i} &= f_{cr,i} - f_{cr,i-1} \end{aligned} \tag{3}$$

3.2.5. Step E: Viscoelastic analysis

Together with the incremental load, the local forces in incremental formulation are applied to the lattice system to simulate the viscoelastic behaviour of a printed structure, as shown in Fig. 4.

3.2.6. Step F: system updates

The nodal displacement derived from Step C is used to update the numerical model. Meanwhile, critical elements whose element stresses (as expressed in Eq. (4)) are higher than material strength (tensile or compressive) are removed. Then, they are replaced by the equivalent forces to consider stress redistribution.

$$\sigma = \alpha_{\mathrm{N}}\frac{F}{A} + \alpha_{\mathrm{M}}\frac{\left(|M_i|, |M_j|\right)_{\max}}{W} \tag{4}$$

Here, F and M represent the uniaxial force and bending moment applied to the lattice element; A and W stand for cross-section and section modulus, respectively. The parameters α_{N} and α_{M} represent the contribution of normal force and bending on element failure. Based on the previous research [55–60], α_{N} equal to 1.0 and α_{M} equal to 0.05 are used herein [61]. These coefficients are based on previous research [60], where it was found to capture experimentally derived failure modes for hardened cementitious materials. Considering this previous finding, we used the same parameters in our previous 3D printing numerical analysis and find they can reproduce the quantified failure modes and determine the critical printing height [12,37,38]. Fig. 5.

3.2.7. Step F: stop criterion

The numerical analysis continues until the failure criterion mentioned in Section 2.1 is met. In that case, the predicted critical printing layer will be given, as well as the failure mode.

4. Results

Here, a numerical study is carried out to evaluate the lattice model with the incorporation of geometric nonlinearity, early-age creep, and localized damage for predicting the buildability of 3DCP. The model performance will be quantified through comparison to a printing experiment, in which the critical printing height and the failure mode were determined.

4.1. Model calibration

3D printable mortar/paste behaves approximately as a visco-elasto-plastic material. After material deposition, the printed segments are at rest [13]. The instantaneous and time-dependent deformation, therefore, determine the structural deformation. The former is associated with the elasto-plastic material behaviour, and the unconfined uniaxial compression/green strength test is commonly used to determine time-dependent stiffness and strength. To describe this viscoelastic behavior, early-age creep tests are performed to provide the creep compliance required in this local force method.

4.1.1. Green strength test

This section gives a brief overview of the model calibration on the early-age material stiffness and strength of 3D printable mortar. The mix composition of 3D printable mortar is given in Table 1. Green strength tests are performed to measure material stiffness and strength at difficult hardening time; the repeated minute-long quasi-static experiments are used to measure early-age creep. Cylindrical specimens with a height of 70 mm and diameter of 70 mm were used, allowing to minimize the occurrence of eccentric loading during testing. These samples were cast, i.e., not printed, so there were no multiple printing layers present in the tested specimens. For the uniaxial compression test, the samples are tested at 20 and 30 min using a hydraulic testing machine (Instron) equipped with a loadcell with 0.1 N loading accuracy. During the test, a loading rate of 0.5 mm/s is used. Detailed information can be found in our previous research [41]. It should be noted that the stiffness derived from the green strength test is notably lower than the elastic modulus measured by unloading tests [41]. This difference can be attributed to the fact that the evaluation of stiffness in the green strength test considers the contribution of plastic deformation.

Based on the green strength tests, the relevant numerical analyses are performed to calibrate the required input parameters for the 3D printing model. In view of computational convenience of solution accuracy, the mesh resolution equal to 1 mm is employed, creating a model composed of 10,255 lattice nodes connected by 74,195 beam elements. Material compressive strength is assumed to be 10 times that of the tensile strength throughout calibration procedure. Details of the calibration process can be found in our previous research [12]. The calibrated time-dependent material properties of lattice elements are expressed as:

$$\begin{aligned} E(t) &= 53 + t \\ f_c(t) &= 20.54 + 0.5{\cdot}t \\ f_t(t) &= 2.054 + 0.05{\cdot}t[\mathrm{kPa}] \end{aligned} \tag{5}$$

Here, t refers to the hardening/printing time (min); E is the material stiffness, i.e., 'elastic modulus' from the green strength test. f_c and f_t refer to the material compressive and tensile strength, respectively.

4.1.2. Early-age creep test

A quasi-static compressive loading-unloading cycle test is conducted to characterize the creep evolution in different aging times. During

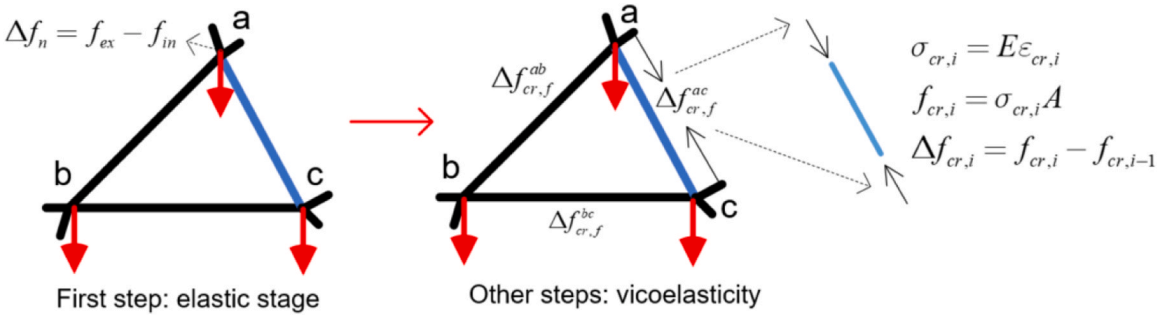

Fig. 4. Viscoelastic analysis of an individual beam element [42].

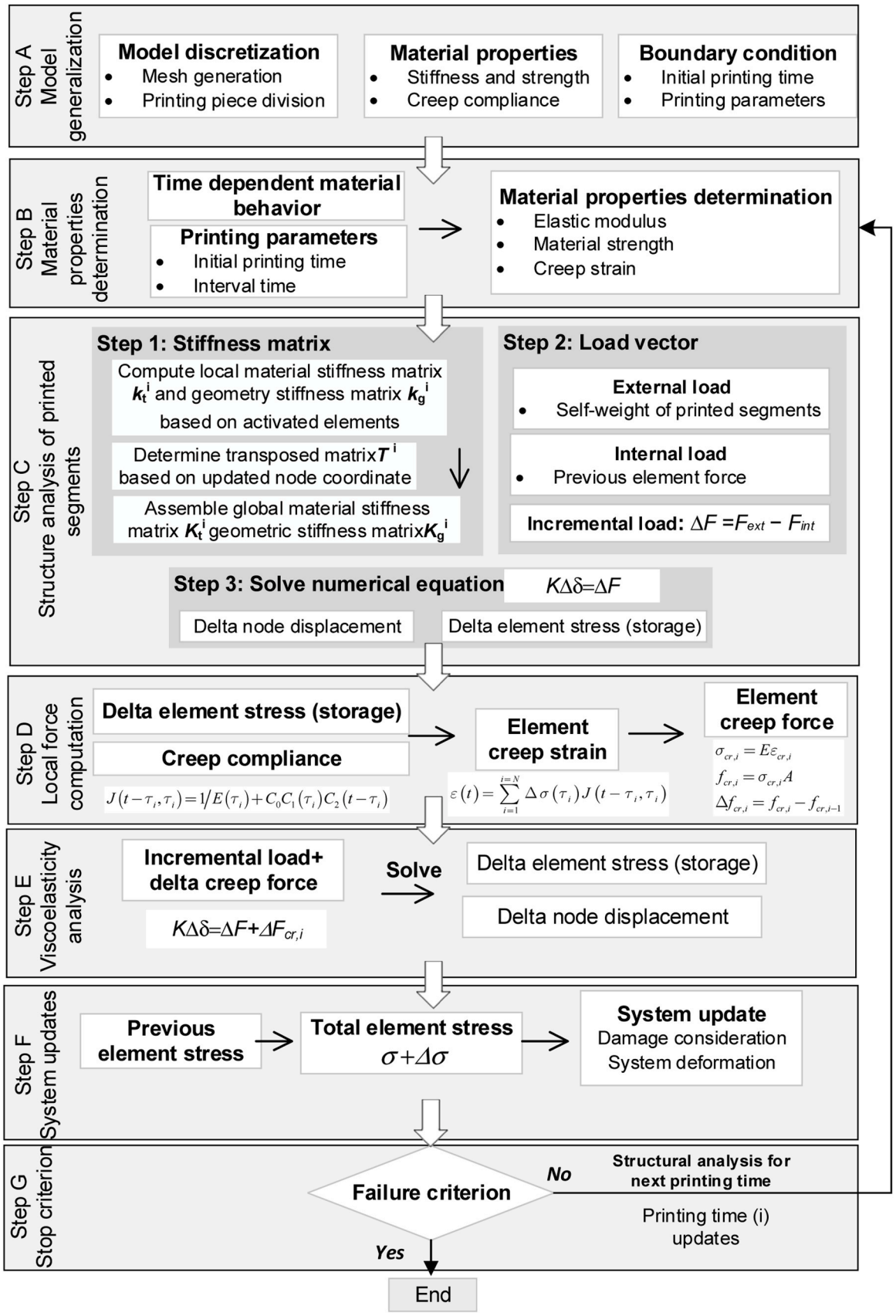

Fig. 5. Flowchart about the 3D printing model with creep consideration.

Table 1
Mix design of 3D printable mortar [kg/m^3] [41].

Cement I 42.5	Water	VMA	Sand (0.01–0.02 mm)	w/c ratio
1140	342	0.83	770	0.3

testing, two environmental factors i.e., RH and temperature, were kept constant to avoid plastic shrinkage. Creep was measured at multiple ages, i.e., $t = 30, 40, 50, 60, 70, 80$ and 90 min. The loading duration for each testing stage is 180 s, in order to minimize the changes of the microstructure during the test. A compressive force of 5 N was adopted to keep the ratio of stress-to -strength below 30% and minimize the impact of localized damage on creep measurement. Furthermore, a loading speed equal to 2.5 N/s was used to ensure that the majority of creep deformation occurs during the constant loading stage and not during the loading stage. A summary of early-age creep tests is given in Fig. 6, a series of creep tests were conducted at different aging times, while maintaining the same loading duration for each test. Loading time refers to the period during which the creep force is applied to the tested sample, while aging time reflects the hydration state at that moment. Each curve in different colors represents a different creep test, and the range of each curve illustrates the duration for which the applied creep load is sustained. Subsequently, the experimental data from a series of aging creep tests are used to fit a creep compliance surface (as shown in Fig. 6). This fitted double power law function (as expressed in Eq. (6)) describes the evolution of creep compliance with the inputs of loading duration and hardening time. This function is then incorporated into the 3D printing model to simulate the viscoelastic behaviour.

$$J\left(t-\tau,\tau\right) = \frac{1}{-22490} + 3574\left(\frac{1}{\tau}\right)^{1.1187}(t-\tau)^{0.1062}\left[1\Big/\mathrm{MPa}\right] \tag{6}$$

4.2. Model validation

A wall structure with 350 mm length, 15 mm width, and 4 mm layer height is employed for buildability quantification with the consideration of early-age creep, as shown in Fig. 7. The printing velocity is set to 600 mm/min in this experiment to avoid instability and tearing of the extruded filament caused by the imbalance speed between nozzle movement and material flow. More detailed information about the 3D printer, printable mortar and printing process can be found in [41].

A numerical model with the wall layout printing geometry is created to simulate the printing experiment. In Fig. 8(a), the colorful cloud represents the different labels assigned to the divided printing segments, which are introduced to account for the non-uniform gravitational loading. It has been shown [12,33] that increasing the number of division segments leads to a reduction in the failure height and eventually converges to a lower-bound value. Considering the computational cost, this numerical model divides each printing layer into three segments (as shown in Fig. 8(b)) to allow for the non-uniform gravitational loading condition caused by the continuous printing process. Besides, the high friction boundary condition is used during structural analysis. To minimize the effects of mesh size, this wall structure uses the same mesh resolution, i.e., 1 mm, the same as used in the computational green strength and early-age creep test. In the end, a wall structure is built, each layer of which is composed of 21,060 lattice nodes connected by 157,950 elements.

The structural analysis for buildability quantification is conducted with the time-dependent material stiffness and strength, as well as creep compliance as inputs. During the printing process, the aging time and loading duration of each segment are calculated in the analysis based on their position in the printing sequence. For example, after three segments have been printed, the initial segment encompasses three aging times, each corresponding to a specific loading duration. The superposition principle is used to compute the creep response. In subsequent segments, such as the second printed segment, there are two aging times and their corresponding loading durations. As the printing progresses and the fourth segment is printed, the previously printed segments will include four aging times and loading durations. The creep response of each segment is calculated using the superposition principle. Corresponding stiffness and strength values are determined based on the relevant printing times.

The critical printing height and the structural failure mode are commonly used criteria for model validation. Lattice modelling of the printing process reproduces the buckling dominant failure mode, which is similar to experimental findings. In Fig. 9, the initial structure is identical to the one shown in Fig. 8(a). For views 1 and 2, the colorful cloud represents the magnitude of structural deformation, calculated using the equation (sqrt(x^2 + y^2 + z^2)). The deformed structure provides insight into the direction of deformation, revealing that the out-of-plane deformation exerts a dominant influence compared to the in-plane deformation. In relation to the buildability quantification, the wall structure fails at the 34th layer due to the out-of-plane displacement in the printing test. In contrast, the lattice model predicts that this wall structure will fail at 32nd layer. There is around 5% difference between the numerical prediction and the experimental result. It can be

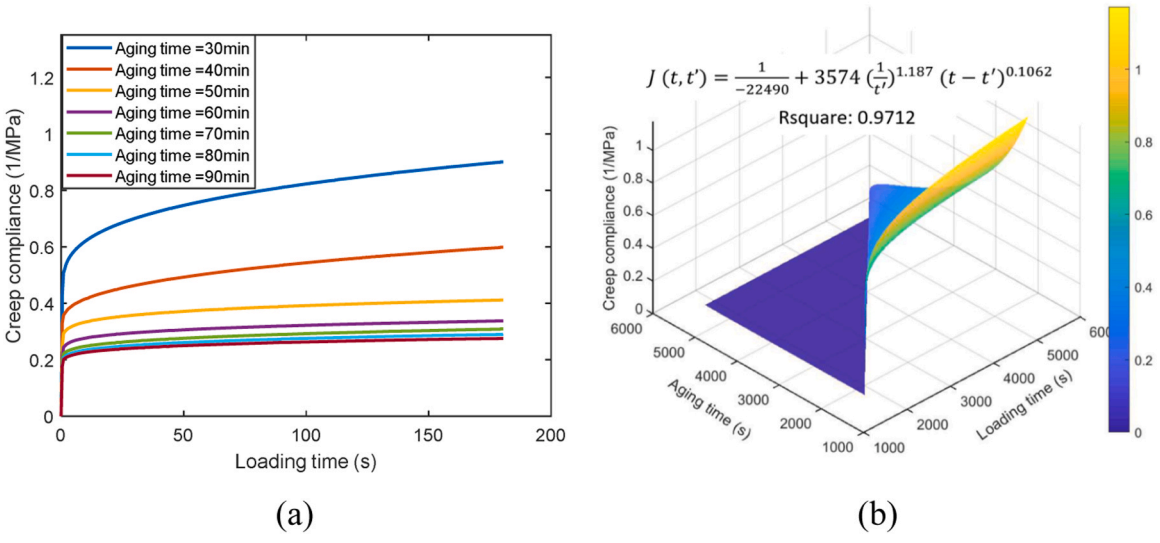

Fig. 6. Fitted creep compliance surface [41] (a) creep evolution at different hardening times (b) fitted creep compliance surface.

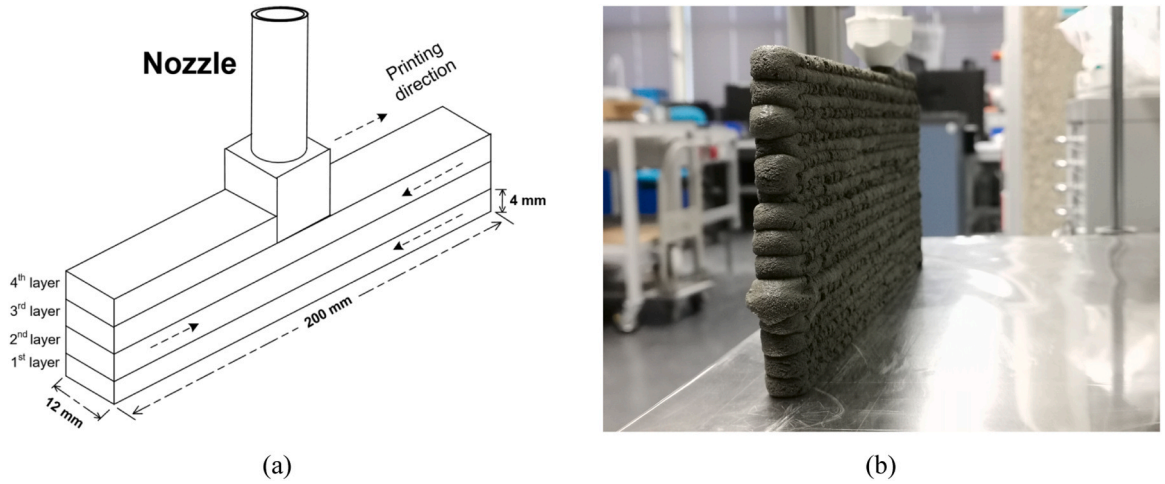

Fig. 7. Wall structure for 3DCP (a) schematic diagram for designed wall structure (b) 3D printing test.

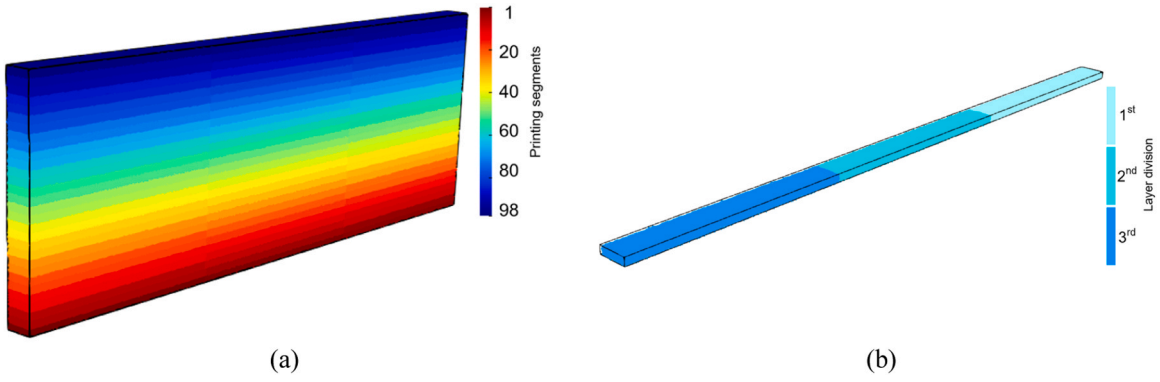

Fig. 8. A numerical model with wall structure for 3DCP (a) layers of numerical model (b) layer division.

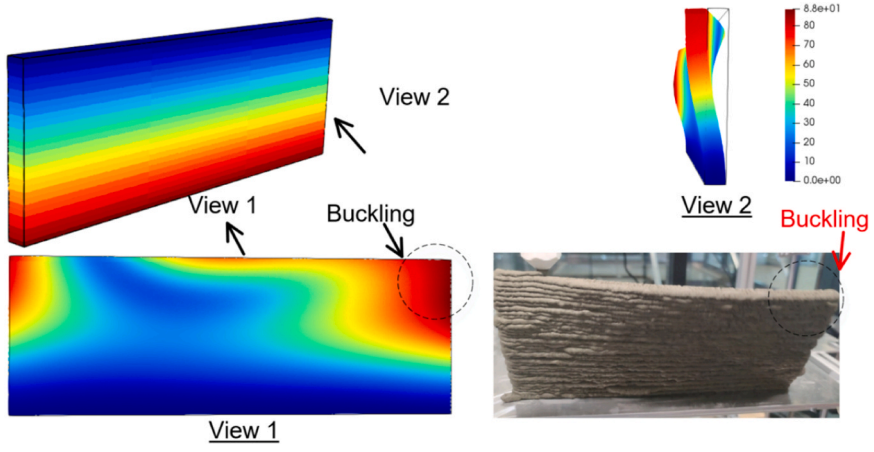

Fig. 9. Failure mode for wall structure from numerical modeling.

inferred that this 3D printing model can reproduce the experimentally derived failure mode and relatively accurately predict the critical printing height.

5. Discussion

Lattice modelling of the wall structure shows similar results the with experimental findings in terms of the critical printing height and the failure mode. The impact of early-age creep on buildability will now be quantitatively analyzed through a variety of printing geometries dominated by different failure modes. In the end, the coupled effect between the early-age creep and localized damage on the structural buildability will be discussed from the perspective of damage generation and creep strain evolution.

5.1. Factors influencing creep compliance at early age

Hardening time, loading duration, and material characteristics are

the main factors that determine the creep compliance. Our previous study [42] demonstrates that the hardening time has a more significant impact on creep prediction of 3D printed segments than loading duration. In this section, we will incorporate the creep compliance function, which includes various aging terms, to examine how it affects structural analysis during 3D printing. Here, simulations with an aging term of 2100 s are regarded as references, which are the same with printing trials conducted in [41]. During the printing trials, the preparation time was 15 min, and the printing process for the cylinder structure took 20 min, and the wall structure required a similar printing time of around 20 min in total. A aging time equal to 35 min (15 +20 min) minutes is adopted for numerical analysis. It is important to note the specific aging time can be adjusted accordingly (e.g., 15 min or 10 min). Using the different 3D printable materials, Esposito et al. [40] also tested early-age creep behaviour of 3D printable mortar, showing that the early-age creep accounts for more than 1% of the overall deformation at resting time equal to 0 min, which is roughly 100 times greater than we have previously observed [41]. This indicates that the material mix design significantly affects the creep strain evolution. The impact of mix design on creep evolution is reflected by the coefficient C_0 in the double power law function. Herein, the creep coefficient C_0 is increased 100 times to investigate the effects of different creep magnitudes (i.e., representative of different mix designs) on buildability quantification.

5.2. Failure modes

This numerical model allows for three typical failure modes: elastic buckling, plastic collapse, and a combination of the two. Previous research [35] has demonstrated that the hollow cylinder structures of varying sizes may show different typical failure modes. For the hollow cylinders with small diameter, the structure generally fails due to material yielding in the bottom zone. As the diameter of the hollow cylinder increases, buckling becomes more prevalent and affects the structural failure mode. The structure failure mode will transition from the plastic collapse to combined and then elastic buckling. To investigate the creep impact of different failure modes, we adopt these specific hollow cylinder geometries in our research, in which the diameter are quite different to reproduce the different failure modes. Based on the literature [35], we expect that the hollow cylinder structure with the smallest diameter to be primarlily influenced by plastic collapse, while the middle section may exhibit a combined failure mode. In the case of the largest hollow cylinder, buckling may become a significant factor contributing to structural failure.

In terms of each printed segment, these numerical cases use the time-dependent material properties expressed in Eq. (5) as well as creep compliance described by Eq. (7). Table 2 summarizes the input parameters and failure information of all simulated cases. Each printing layer is divided into 4 printed segments for non-uniform gravitational loading consideration. The failure step, failure mode, and deformed structure are provided to quantify the creep impact on 3D printing simulation. It should be noted that the failure step in this research refers to the critical printing step, in which the analyzed object reaches the structural failure criterion and fails.

$$J\left(t-\tau,\tau\right)=\frac{1}{-22470}+23260\left(\frac{1}{\tau}\right)^{1.363}(t-\tau)^{0.1167}\left[1\Big/\mathrm{MPa}\right] \tag{7}$$

5.3. Numerical results

Fig. 10 shows the failure modes of all cases listed in Table 2. Fig. 11 (a) illustrates the gradual increase in system deformation accompanied by localized damage, which indicates a typical plastic collapse dominant failure. In Fig. 11 (b), it can be observed that the materials near the bottom yield, while local buckling occurs in the top area, suggesting the presence of a combined failure mode. Additionally, in Fig. 11 (c) sudden local buckling leads to extensive damage, confirming the occurrence of elastic buckling. These numerical results provide solid evidence that the expected failure modes are successfully produced. These results confirm that the quantitative impact of early age creep on buildability quantification in geometries dominated by different failure modes can be further investigated.

When comparing the numerical examples with or without creep (i.e., 1 and 3, 5 and 7, as well as 9 and 11), it can be seen that the creep effect on structural analysis of 3DCP can be ignored in the context of this 3D printable material. In terms of the impact of aging term, the failure steps obtained from numerical cases (i.e., 2, 6 and 10) indicate that the creep behaviors with smaller aging term make the designed structures easier to fail. Although this difference (i.e., 0%, 0.6% and 0.81%) is small, structures in which plastic collapse is the dominant failure mode are affected more than those in which buckling is dominant. When comparing the same geometries with different creep coefficients C_0, significant differences (i.e., 46.99, 62.6% and 14.29%) in critical printing height can be found. Fig. 10 shows the numerical cases with amplified creep coefficient C_0 result in different failure models compared to other cases. This shows that the impact of creep on the structural buildability differs depending on the printing material used (and its creep). It can be concluded that early-age creep must be considered for buildability quantification of 3DCP for printable materials with high creep.

Comparing the numerical cases (i.e., 4, 8 and 12) with amplified creep deformation with the reference ones (i.e., 3, 7 and 11), Fig. 12 shows the deformed shape of hollow cylinder structures under different printing steps. Fig. 13 provides the damage information for structural analysis during the printing process. The numerical cases with larger creep coefficients result in more localized damage. As a result, a lower

Table 2
Summary of numerical cases for creep analysis.

Case	Geometry	Size (mm)			Creep		Failure mode	Failure step	Difference (%)
		Length/ Diameter	Width	Layer height	Aging term (s)	C_0			
1	Hollow cylinder	100	12	12	No creep	0	Plastic collapse	166	0
2					36	1		165	0.6%
3					2100	1		166	Ref
4					2100	100		88	46.99%
5		200	12	12	No creep	0	Combined failure mode	123	0
6					36	1		122	0.81%
7					2100	1		123	0
8					2100	100		79	35.77%
9		400	12	12	No creep	0	Elastic buckling	70	0
10					36	1		70	0
11					2100	1		70	Ref
12					2100	100		60	14.29%

* Difference refers to the deviation between the reference model with the analyzed one.

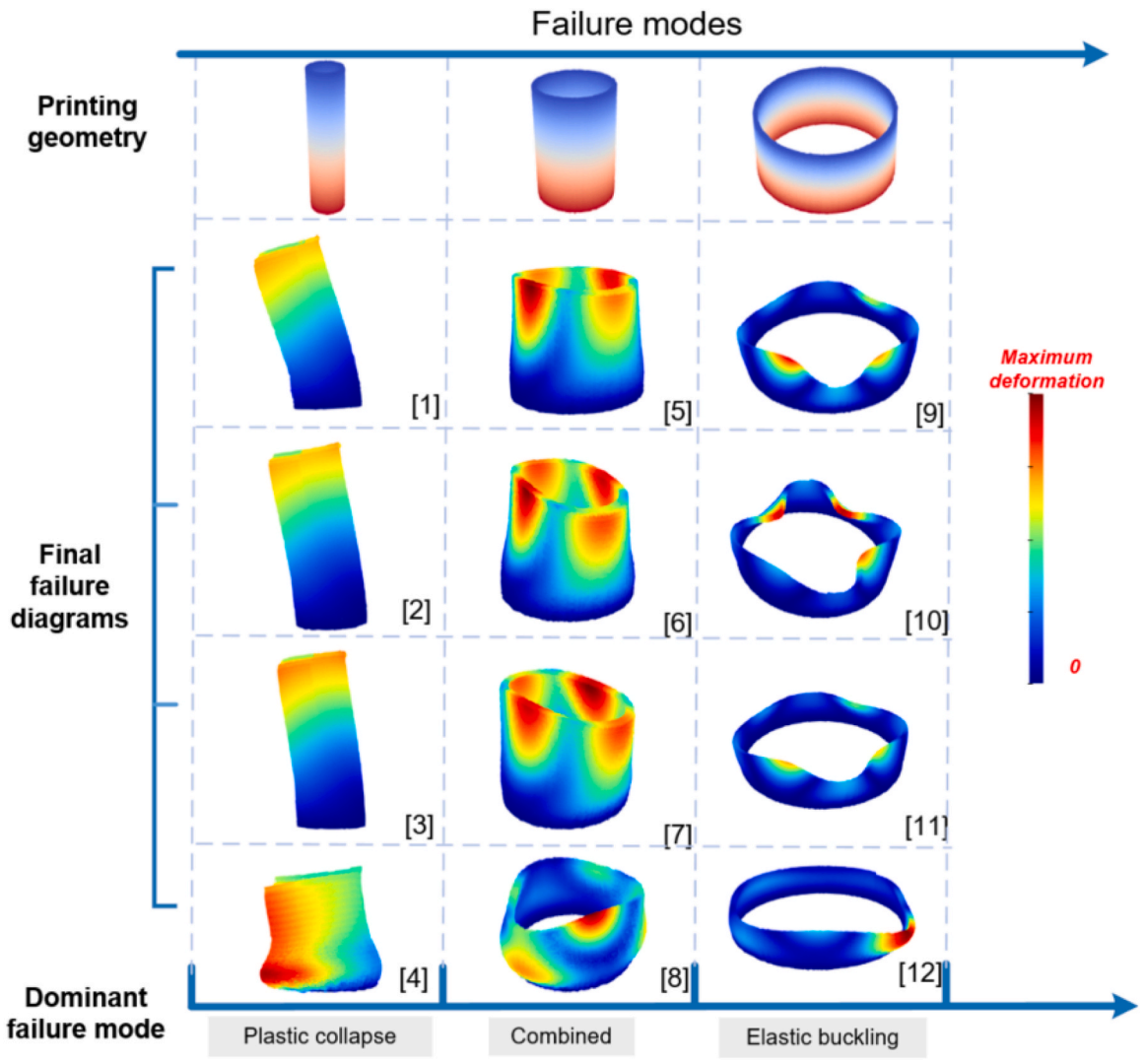

Fig. 10. Failure modes of listed numerical cases (case number is given in parentheses).

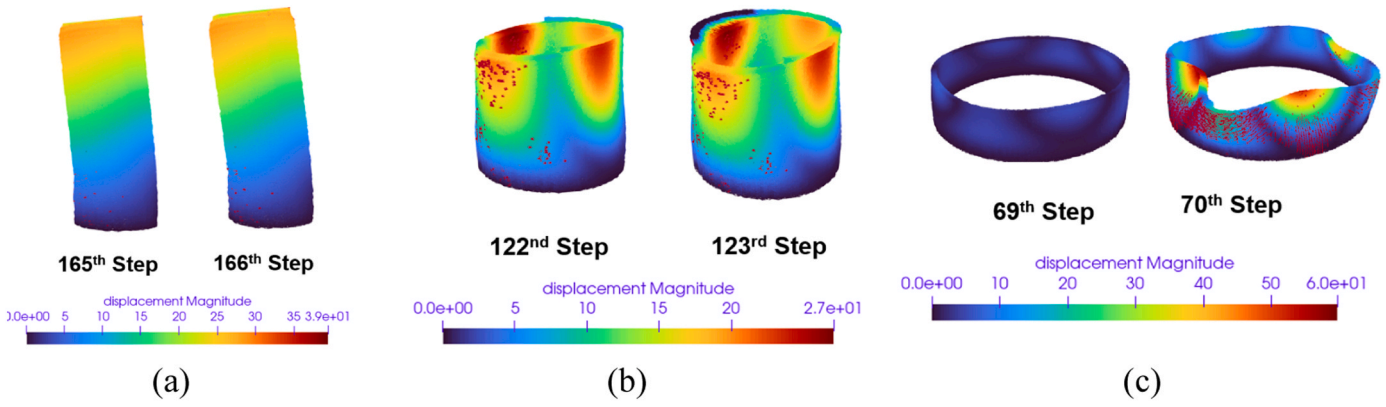

Fig. 11. Three typical failure modes during printing process (a) plastic collapse; (b) combined failure; (c) elastic buckling (red points indicating localized damage).

critical printing height is found. In contrast to material yielding dominant failure mode, the buckling determined failure geometry is less affected by creep deformation. This is because the material stiffness instead of the strength determines the critical printing height for such kind of printing structure.

In contrast, the numerical results indicate that the influence of early-age creep on structural deformation or the reference cases (i.e., 3, 7 and 11) is limited. A possible reason is that the early-age creep strain of this kind of printable material is so small that its impact on structural deformation can be neglected. Fig. 14 shows a ratio between the creep to total strain for all beam elements during the numerical analysis for case 3. This small ratio (i.e., roughly 1%) suggests that there is a limited

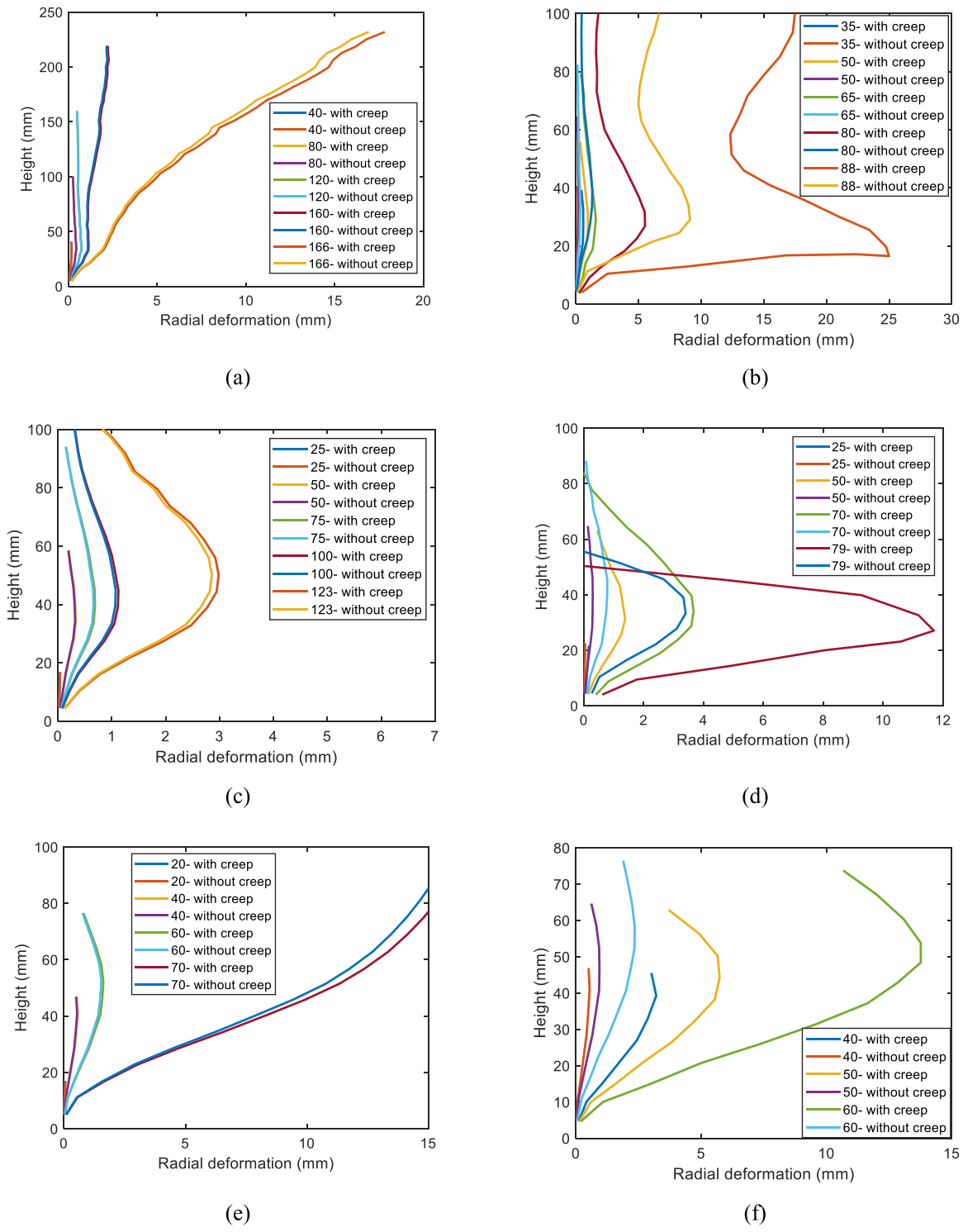

Fig. 12. Radial deformation versus height (a) case 3; (b) case4; (c) case 7; (d) case 8; (e) case 11; (f) case 12.

contribution from early-age creep to the total deformation. Fig. 15 shows the evolution of creep in a randomly chosen element during the structural analysis. Although creep in this lattice element increases during the numerical analysis, the creep strain is still limited until the system eventually fails. As a result, the buildability and the structural deformation of 3DCP remain almost unchanged with the consideration of early-age creep.

During the numerical analysis, positive incremental element stresses (namely, tensile stress) can sometimes be observed (as shown in Fig. 15 (a)), which means that this selected element is sometimes exposed to the incremental tensile stress. This is because the continuous extrusion process results in some printed segments being subjected to different loading conditions (namely, loading and unloading situations). This requires the model to account for the loading-unloading on the element scale. Our previous research has demonstrated that the 'local force method' [42] can mimic the creep behaviour under various loading conditions. Thus, the creep impact of buildability quantitation of 3DCP can be accurately analyzed.

The numerical cases presented above demonstrate that material properties play a crucial role in determining the creep response for

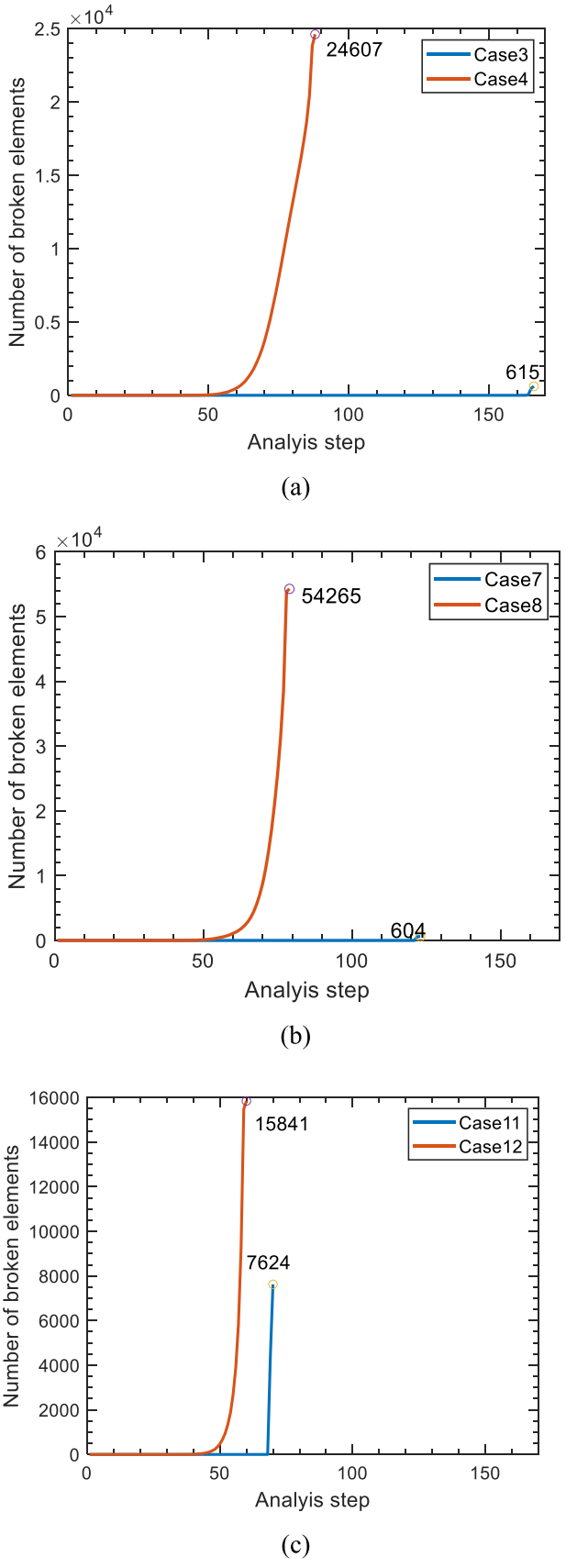

Fig. 13. Damage information during numerical analysis for different failure modes (a) plastic collapse (b) combined failure mode (c) elastic buckling.

quantifying buildability. To provide a comprehensive analysis, additional creep coefficients (specifically 10, 25, 50, and 75) were used in the numerical analyses. These coefficients were used to conduct further investigations, and the results are now included in Table 3. The impact of these additional coefficients on the findings was explored and visualized in Fig. 16.

By expanding the range of creep coefficients, our objective was to enhance the understanding of how different creep levels influence the structural behavior. Our observations indicate that an increase in the creep parameters (C_0) leads to a decrease in the critical printing height across all failure modes. This decrease is attributed to the amplified creep, which induces additional deformation in the printed system, ultimately resulting in structural failure.

Fig. 16 illustrates that the failure mode most affected by increased creep is plastic collapse, whereas elastic buckling is the least affected. This phenomenon can be explained by the fact that elastic buckling is primarily influenced by the stiffness of the system. Although increased creep causes more damage, the newly generated damage is overshadowed by the impact of buckling.

6. Conclusions

Herein, the local force method is incorporated into a previously proposed model for concrete 3D printing to investigate the influence of early-age creep on buildability. The green strength and early-age creep tests are first used to characterize the visco-elasto-plastic material properties of lattice elements. A printing experiment is then utilized to validate the model. Finally, a series of parametric analyses are performed to examine how early-age creep affects the structural analysis of 3DCP, ranging from critical printing height, failure mode, and structural deformation. This research yields the following insights and conclusions:

- The structural failure during printing process are codetermined by the material properties and designed geometry. Identifying material yielding and local buckling as essential factors in simulating different failure modes, including elastic buckling, plastic collapse and combined one.
- The influence of aging time on structural analysis has revealed that structures with earlier aging time are more prone to failure, leading to lower failure heights. Nonetheless, the effect of aging time is limited as the primary factor determining structural deformation is elasto-plastic deformation rather than creep. Structures that are predominantly governed by plastic collapse are more significantly impacted compared to those influenced by buckling. These findings emphasize the importance of considering the role of hardening time in analyzing structural behavior and failure mechanisms.
- The impact of creep on the structural buildability is dependent on the printing material used. When a significant creep compliance (i.e., C_0) is incorporated into the 3D printing model, the critical printed height decreases significantly. This decrease is primarily attributed to the high creep, which introduces additional deformation in the printed system and ultimately leads to structural failure. Structures that are susceptible to elastic buckling exhibit similar buildability even with high creep, with the failure mode remaining unchanged. This is because that system stiffness outweighing the newly generated damage caused by increased creep. On the other hand, structures prone to plastic collapse experience reduced buildability and a shift in the failure mode. These findings highlight the importance of considering the influence of creep when assessing the buildability and failure behavior of 3D-printed structures, particularly for those susceptible to plastic collapse.

This model allows considering the effects of early-age creep during the printing process. Further improvements can be made by incorporating the effect of cold joints, moisture transfer and thermal transport

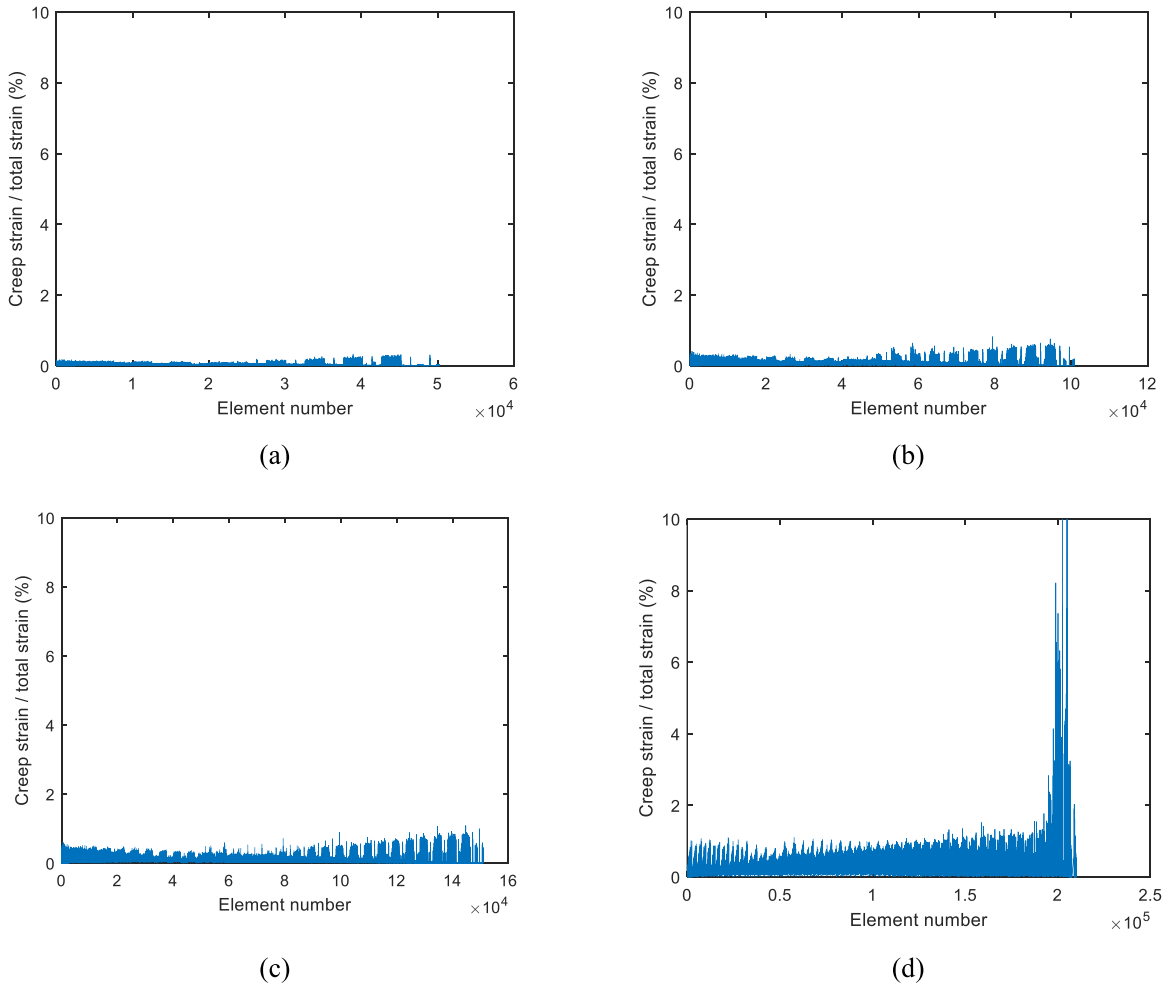

Fig. 14. Creep strain observation during numerical analysis (a) 40 step (b) 80 step (c) 120 step (d) 166 step.

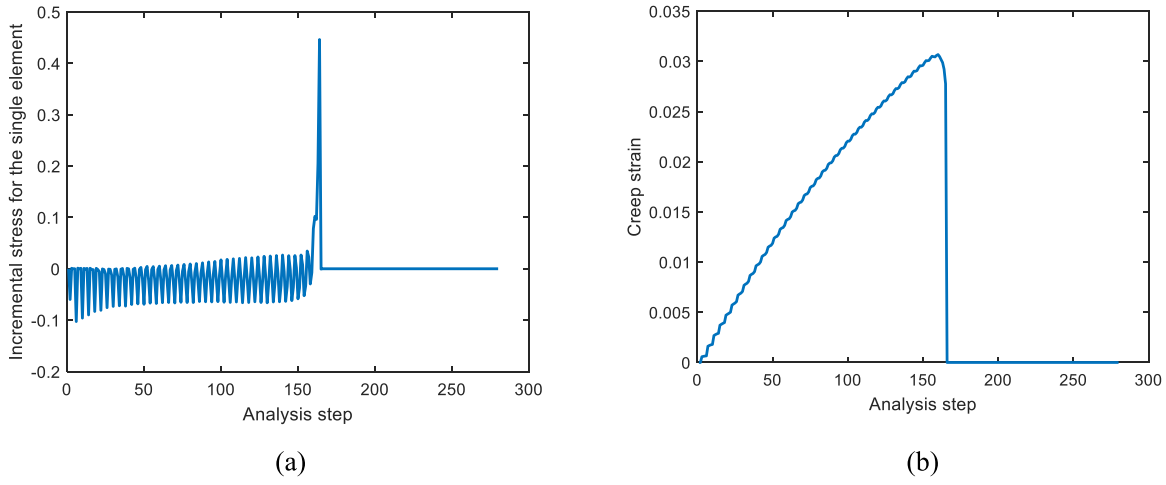

Fig. 15. Creep behaviour of randomly picked lattice element (a) incremental element stress (b) creep evolution.

into the model.

CRediT authorship contribution statement

Minfei Liang: Writing – review & editing, Methodology. **Yu Chen:** Writing – review & editing, Methodology. **Erik Schlangen:** Writing – review & editing, Supervision, Methodology, Investigation, Conceptualization. **Branko Šavija:** Writing – review & editing, Supervision, Methodology, Investigation, Conceptualization. **Ze Chang:** Writing – original draft, Software, Methodology, Investigation, Formal analysis, Conceptualization.

Table 3
Summary of numerical cases for creep analysis.

Case	Geometry	Size (mm)				Failure mode	Failure step	Difference (%)
		Length/ Diameter	Width	Layer height	C_0			
3	Hollow cylinder	100	12	12	1	Plastic collapse	166	Ref
13					10		165	0.60
14					25		150	9.64
15					50		118	28.92
16					75		101	39.16
4					100		88	46.99
7		200	12	12	1	Combined failure mode	123	Ref
17					10		123	0.00
18					25		118	4.07
19					50		100	18.70
20					75		88	28.46
8					100		79	35.77
11		400	12	12	1	Elastic buckling	70	Ref
21					10		70	0.00
22					25		70	0.00
23					50		69	1.43
24					75		66	5.71
12					100		60	14.29

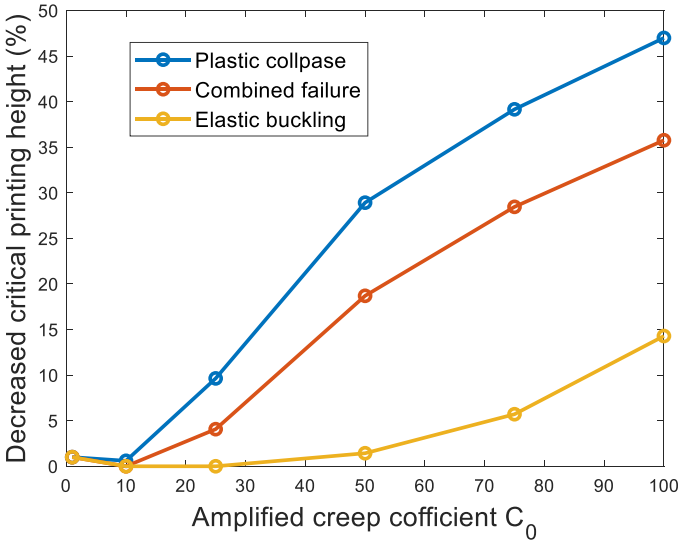

Fig. 16. The relationship between the amplified creep coefficient C_0 with decreased critical printing height.

Declaration of Competing Interest

The authors declare that they have no known competing financial interests or personal relationships that could have appeared to influence the work reported in this paper.

Data Availability

Data will be made available on request.

Acknowledgements

This work was supported by the China Scholarship Council [201806060129, Ze Chang; 202007000027, Minfei Liang] and the European Research Council (ERC) within the framework of the ERC Starting Grant Project "Auxetic Cementitious Composites by 3D printing (ACC-3D)", Grant Agreement Number 101041342 [Branko Šavija].

References

[1] F. Bos, R. Wolfs, Z. Ahmed, T. Salet, Additive manufacturing of concrete in construction: potentials and challenges of 3D concrete printing, Virtual Phys. Prototyp. 11 (3) (2016) 209–225.
[2] C. Gosselin, R. Duballet, P. Roux, N. Gaudillière, J. Dirrenberger, P. Morel, Large-scale 3D printing of ultra-high performance concrete – a new processing route for architects and builders, Mater. Des. 100 (2016) 102–109.
[3] A. Kazemian, X. Yuan, E. Cochran, B. Khoshnevis, Cementitious materials for construction-scale 3D printing: laboratory testing of fresh printing mixture, Constr. Build. Mater. 145 (2017) 639–647.
[4] B. Nematollahi, M. Xia, J. Sanjayan, Current progress of 3D concrete printing technologies, Proc. 34th Int. Symp. . Autom. Robot. Constr. (ISARC) (2017).
[5] R.A. Buswell, W.L. de Silva, S. Jones, J. Dirrenberger, 3D printing using concrete extrusion: a roadmap for research, Cem. Concr. Res. 112 (2018) 37–49.
[6] R. Comminal, W.R.L. da Silva, T.J. Andersen, H. Stang, J. Spangenberg, Modelling of 3D concrete printing based on computational fluid dynamics, Cem. Concr. Res. 138 (2020), 106256.
[7] V. Mechtcherine, F.P. Bos, A. Perrot, W.L. da Silva, V. Nerella, S. Fataei, R.J. Wolfs, M. Sonebi, N. Roussel, Extrusion-based additive manufacturing with cement-based materials–Production steps, processes, and their underlying physics: a review, Cem. Concr. Res. 132 (2020), 106037.
[8] M.S. Khan, F. Sanchez, H. Zhou, 3-D printing of concrete: beyond horizons, Cem. Concr. Res. 133 (2020), 106070.
[9] M.T. Mollah, R. Comminal, M.P. Serdeczny, D.B. Pedersen, J. Spangenberg, Stability and deformations of deposited layers in material extrusion additive manufacturing, Addit. Manuf. (2021), 102193.
[10] M.P. Serdeczny, R. Comminal, D.B. Pedersen, J. Spangenberg, Numerical simulations of the mesostructure formation in material extrusion additive manufacturing, Addit. Manuf. 28 (2019) 419–429.
[11] R.J. Wolfs, T.A. Salet, N. Roussel, Filament geometry control in extrusion-based additive manufacturing of concrete: The good, the bad and the ugly, Cem. Concr. Res. 150 (2021), 106615.
[12] Z. Chang, Y. Xu, Y. Chen, Y. Gan, E. Schlangen, B. Šavija, A discrete lattice model for assessment of buildability performance of 3D-printed concrete, Comput. Civ. Infrastruct. Eng. 36 (5) (2021) 638–655.
[13] N. Roussel, Rheological requirements for printable concretes, Cem. Concr. Res. 112 (2018) 76–85.
[14] F.A. Cardoso, V.M. John, R.G. Pileggi, Rheological behavior of mortars under different squeezing rates, Cem. Concr. Res. 39 (9) (2009) 748–753.
[15] M. Chen, L. Li, Y. Zheng, P. Zhao, L. Lu, X. Cheng, Rheological and mechanical properties of admixtures modified 3D printing sulphoaluminate cementitious materials, Constr. Build. Mater. 189 (2018) 601–611.
[16] H. Jeong, S.-J. Han, S.-H. Choi, Y.J. Lee, S.T. Yi, K.S. Kim, Rheological property criteria for buildable 3D printing concrete, Materials 12 (4) (2019) 657.
[17] R. Jayathilakage, J. Sanjayan, P. Rajeev, Direct shear test for the assessment of rheological parameters of concrete for 3D printing applications, Mater. Struct. 52 (1) (2019) 1–13.
[18] Y. Zhang, Y. Zhang, W. She, L. Yang, G. Liu, Y. Yang, Rheological and harden properties of the high-thixotropy 3D printing concrete, Constr. Build. Mater. 201 (2019) 278–285.
[19] J. Kruger, S. Zeranka, G.J.C. van Zijl, B. Materials, An ab initio approach for thixotropy characterisation of (nanoparticle-infused) 3D printable concrete, 224 (2019) 372–386.
[20] J. Kruger, S. Zeranka, G.J.Ai.C. van Zijl, 3D concrete printing: a lower bound analytical model for buildability performance quantification, 106 (2019) 102904.

[21] J. Kruger, A. du Plessis, G. van Zijl, An investigation into the porosity of extrusion-based 3D printed concrete, Addit. Manuf. 37 (2021), 101740.
[22] B. Panda, C. Unluer, M.J. Tan, Investigation of the rheology and strength of geopolymer mixtures for extrusion-based 3D printing, Cem. Concr. Compos. 94 (2018) 307–314.
[23] J. Kruger, S. Zeranka, G. van Zijl, Quantifying constructability performance of 3D concrete printing via rheology-based analytical models. Rheology and Processing of Construction Materials, Springer, 2019, pp. 400–408.
[24] M. Briffaut, F. Benboudjema, J.-M. Torrenti, G. Nahas, Concrete early age basic creep: experiments and test of rheological modelling approaches, Constr. Build. Mater. 36 (2012) 373–380.
[25] Y. Qian, S. Kawashima, Use of creep recovery protocol to measure static yield stress and structural rebuilding of fresh cement pastes, Cem. Concr. Res. 90 (2016) 73–79.
[26] J. Kruger, S. Zeranka, G. van Zijl, 3D concrete printing: a lower bound analytical model for buildability performance quantification, Autom. Constr. 106 (2019), 102904.
[27] A.S.J. Suiker, Mechanical performance of wall structures in 3D printing processes: theory, design tools and experiments, Int. J. Mech. Sci. 137 (2018) 145–170.
[28] R. Wolfs, A. Suiker, Structural failure during extrusion-based 3D printing processes, Int. J. Adv. Manuf. Technol. 104 (1–4) (2019) 565–584.
[29] A.S. Suiker, R.J. Wolfs, S.M. Lucas, T.A. Salet, Elastic buckling and plastic collapse during 3D concrete printing, Cem. Concr. Res. 135 (2020), 106016.
[30] R. Wolfs, F. Bos, T. Salet, Early age mechanical behaviour of 3D printed concrete: numerical modelling and experimental testing, Cem. Concr. Res. 106 (2018) 103–116.
[31] R. Wolfs, F. Bos, T.J.C. Salet, Triaxial compression testing on early age concrete for numerical analysis of 3D concrete printing, Cem. Concr. Compos. 104 (2019), 103344.
[32] G. Vantyghem, T. Ooms, W. De Corte, arXiv preprint, arXiv:.06907 (, FEM Model. Tech. Simul. 3D Concr. Print. (2020).
[33] T. Ooms, G. Vantyghem, R. Van Coile, W. De Corte, A parametric modelling strategy for the numerical simulation of 3D concrete printing with complex geometries, Addit. Manuf. 38 (2021), 101743.
[34] Q. Wang, X. Ren, J. Li, A Chemo-Mechanical Model for Predicting the Buildability of 3d Printed Concrete, Available at SSRN 4147420.
[35] G. Vantyghem, T. Ooms, W. De Corte, VoxelPrint: a grasshopper plug-in for voxel-based numerical simulation of concrete printing, Autom. Constr. 122 (2021), 103469.
[36] B. Nedjar, On a geometrically nonlinear incremental formulation for the modeling of 3D concrete printing, Mech. Res. Commun. 116 (2021), 103748.
[37] Z. Chang, M. Liang, Y. Xu, E. Schlangen, B. Šavija, 3D concrete printing: Lattice modeling of structural failure considering damage and deformed geometry, Cem. Concr. Compos. (2022), 104719.
[38] Z. Chang, H. Zhang, M. Liang, E. Schlangen, B. Šavija, Numerical simulation of elastic buckling in 3D concrete printing using the lattice model with geometric nonlinearity, Autom. Constr. 142 (2022), 104485.
[39] Y. Chen, Z. Li, S. Chaves Figueiredo, O. Çopuroğlu, F. Veer, E. Schlangen, Limestone and calcined clay-based sustainable cementitious materials for 3D concrete printing: a fundamental study of extrudability and early-age strength development, Appl. Sci. 9 (9) (2019) 1809.
[40] L. Esposito, L. Casagrande, C. Menna, D. Asprone, F. Auricchio, Early-age creep behaviour of 3D printable mortars: experimental characterisation and analytical modelling, Mater. Struct. 54 (6) (2021) 1–16.
[41] Z. Chang, M. Liang, Y. Xu, Z. Wan, E. Schlangen, B. Šavija, Early-age creep of 3D printable mortar: experiments and analytical modelling, Cem. Concr. Compos. 138 (2022).
[42] Z. Chang, M. Liang, S. He, E. Schlangen, B. Šavija, Lattice modelling of early-age creep of 3D printed segments with the consideration of stress history, Submitted for publication, 2022.
[43] H. Ye, Creep mechanisms of calcium–silicate–hydrate: an overview of recent advances and challenges, Int. J. Concr. Struct. Mater. 9 (4) (2015) 453–462.
[44] D.-T. Nguyen, R. Alizadeh, J.J. Beaudoin, P. Pourbeik, L. Raki, Microindentation creep of monophasic calcium–silicate–hydrates, Cem. Concr. Compos. 48 (2014) 118–126.
[45] A. Shukla, Y.M. Joshi, Boltzmann superposition principle for a time-dependent soft material: assessment under creep flow field, Rheol. Acta 56 (11) (2017) 927–940.
[46] B.T. Tamtsia, J.J. Beaudoin, Basic creep of hardened cement paste A re-examination of the role of water, Cem. Concr. Res. 30 (9) (2000) 1465–1475.
[47] Z.P. Bazant R. L'Hermite Math. Model. creep shrinkage Concr. 1988.
[48] Z.P. Bažant, Prediction of concrete creep and shrinkage: past, present and future, Nucl. Eng. Des. 203 (1) (2001) 27–38.
[49] Z.P. Bažan, Prediction of concrete creep effects using age-adjusted effective 69 (4) (1972) 212–217.
[50] C. Européen, Eurocode 2: Design of concrete structures—part 1-1. General rules and rules for buildings, British Standard Institution, London, 2004.
[51] A.C.J.A. R-08, Guide for modeling and calculating shrinkage and creep in hardened concrete, American Concrete Institute,, Farmington Hills, MI, 2008.
[52] P. Rossi, J.-L. Tailhan, F. Le Maou, L. Gaillet, E. Martin, Basic creep behavior of concretes investigation of the physical mechanisms by using acoustic emission, Cem. Concr. Res. 42 (1) (2012) 61–73.
[53] M.F. Ruiz, A. Muttoni, P.G. Gambarova, Relationship between nonlinear creep and cracking of concrete under uniaxial compression, J. Adv. Concr. Technol. 5 (3) (2007) 383–393.
[54] Z.P. Bažant, B. H, Crack band theory for fracture of concrete, Matér. Et. Constr. 16 (3) (1983) 22.
[55] M. Vassaux, F. Ragueneau, B. Richard, A. Millard, Compressive behavior of a lattice discrete element model for quasi-brittle materials, Comput. Model. Concr. Struct. 1 (2014) 335–344.
[56] E. Schlangen, Experimental and numerical analysis of fracture processes in concrete, Delft University of Technology, Delft, The Netherlands, 1993.
[57] Z. Qian, Multiscale modeling of fracture processes in cementitious materials, Delft University of Technology, Delft, The Netherlands, 2012.
[58] Z. Qian, E. Schlangen, G. Ye, K. van Breugel, Modeling framework for fracture in multiscale cement-based material structures, Materials 10 (6) (2017).
[59] H. Zhang, B. Šavija, S. Chaves Figueiredo, M. Lukovic, E. Schlangen, Microscale Testing and Modelling of Cement Paste as Basis for Multi-Scale Modelling, Mater. (Basel) 9 (11) (2016).
[60] Z. Chang, H. Zhang, E. Schlangen, B. Šavija, Lattice Fracture Model for Concrete Fracture Revisited: Calibration and Validation, Appl. Sci. 10 (14) (2020) 4822.
[61] G. Lilliu, J.G. van Mier, 3D Lattice Type Fract. Model Concr. 70 (7–8) (2003) 927–941.